Effects of clouds, sea surface temperature, and its diurnal variation on precipitation efficiency*

Shen Xin-Yong(沈新勇)[a)†], Qing Tao(庆 涛)[a)], and Li Xiao-Fan(李小凡)[b)]

[a)] *Key Laboratory of Meteorological Disaster of Ministry of Education, Nanjing University of Information Science and Technology, Nanjing* 210044, *China*
[b)] *NOAA/NESDIS/Center for Satellite Applications and Research, College Park, Maryland* 20740, *USA*

(Received 1 November 2012; revised manuscript received 30 January 2013)

The effects of clouds, sea surface temperature, and its diurnal variation on precipitation efficiency are investigated using grid-scale data from nine equilibrium sensitivity cloud-resolving model experiments driven without large-scale vertical velocity. The precipitation efficiencies are respectively defined in surface rainfall, cloud, and rain microphysical budgets. We mathematically and physically demonstrate the relationship between these precipitation efficiencies. The 2 °C increases in spatiotemporal invariant sea surface temperature (SST) from 27 °C to 29 °C and from 29 °C to 31 °C, and the inclusion of diurnal SST difference 1 °C and the 1 °C increase in diurnal SST difference generate opposite changes in the precipitation efficiency by changing ice cloud–radiation interactions. The radiative and microphysical processes of ice clouds have opposite effects on the precipitation efficiency because of the rainfall increase associated with the reduction in the saturation mixing ratio caused by the exclusion of radiative effects and the decrease in rainfall related to the reduction in net condensation caused by the exclusion of deposition processes. The radiative effects of water clouds on the precipitation efficiency are statistically insensitive to the radiative effects of ice clouds.

Keywords: sea surface temperature, diurnal variations, clouds, precipitation efficiency

PACS: 42.68.Ge, 92.60.N–, 92.60.jf, 92.60.Wc **DOI:** 10.1088/1674-1056/22/9/094213

1. Introduction

Precipitation efficiency (PE) has been studied for decades[1–8] since Braham first introduced the concept with the calculation of rainfall source from the inflow of water vapor into the precipitation system through the cloud base more than half a century ago.[9] Over a long period, the PE calculations show negative values due to the inclusion of rainfall sink as well as values higher than 100% due to the exclusion of some rainfall sources. Sui *et al.*[10] calculated large-scale PE (LSPE) and cloud microphysics PE (CMPE) in the surface rainfall budget proposed by Gao *et al.*[11] and the cloud budget, respectively, by excluding all rainfall sinks and including all rainfall sources, which leaded to a normal range of PE in 0%–100%. Gao and Li[12] unified the PE calculation by arguing that the true PE should be defined in the primitive budget in which the precipitation rate is an explicit term and that the true PE should be calculated from grid-scale simulation data due to the high spatial-scale dependent precipitation. This original budget in cloud-resolving model simulation is the rain microphysical budget, and the defined PE is called a rain-microphysics PE (RMPE). Gao and Li[12] found a large difference between RMPE and LSPE and concluded that the water vapor process data cannot be used to estimate the PE. However, the rainfall sources are different in different budgets. The rainfall sources come from atmospheric drying, water vapor convergence, surface evaporation, and hydrometeor loss/convergence in the surface rainfall budget, from vapor condensation and deposition and hydrometeor loss/convergence in the cloud microphysical budget, and primarily from the collection of cloud water by rain and the melting of precipitation ice in the rain microphysical budget. Thus, different rainfall sources with the same rain rate produce different PEs.

From the calculations of PEs with grid-scale simulation data during TOGA COARE by Gao and Li,[12] we find that CMPE is higher than LSPE, but is lower than RMPE. Because non-zero large-scale forcing is much affected by the sea surface temperature (SST) and cloud processes are imposed in the model during the COARE integration, we analyze the equilibrium data from model simulations driven without large-scale vertical velocity in this study. One objective of this study is to mathematically and physically demonstrate that the relationship LSPE<CMPE<RMPE is generally valid in precipitation systems (Section 3). Ping *et al.*,[13] Zhou and Li,[14] and Gao and Li[15] showed that the SST and its diurnal variation as well as cloud radiative and microphysical processes affect the time-mean equilibrium rain rate. Thus, the other objective of this study is to investigate the effects of clouds and SST and its

*Project supported by the National Basic Research Program of China (Grant Nos. 2013CB430103 and 2011CB403405), the National Natural Science Foundation of China (Grant Nos. 41075039 and 41175065), and the Priority Academic Program Development of Jiangsu Higher Education Institutions, China (Grant No. PAPD2 011).

†Corresponding author. E-mail: shenxy@nuist.edu.cn

diurnal variation on PE, which are analyzed in Section 4. The model and experiments will be discussed in Section 2. A summary is given in Section 5.

2. Model and experiments

The data analyzed in this study are cited from nine simulations by Gao *et al.*,[16] Ping *et al.*,[13] and Gao,[17] who used a two-dimensional cloud-resolving model developed by Soong and Ogura,[18] Soong and Tao,[19] and Tao and Simpson,[20] and modified by Li *et al.*[21,22] and Sui *et al.*[23,24] The previous studies[8,25–29] have shown the similarities in terms of collective thermodynamic feedback effect, vertical transports of mass, sensible heat, moisture, thermodynamic field, surface heat flux, surface precipitation, and precipitation efficiency. The nine sensitivity experiment setups are summarized in Table 1. The model is driven by uniformly zonal wind of 4 m·s^{-1} only and is integrated for 40 d to reach a quasi-equilibrium state. The integration data of the last 10 d are used for analysis in this study. The set of equilibrium simulation data has been used to study the effects of sea surface temperature and its diurnal variation on rainfall,[14,30,31] radiative and microphysical effects on rainfall,[13] diurnal rainfall cycle,[32–35] the role of surface evaporation in rainfall process,[36] effects of SST, clouds and diurnal variation on the vertical temperature structure,[37,38] and rainfall separation.[39,40]

Table 1. Summary of sensitivity experiments.

Experiment	SST	Radiation	Ice microphysics
SST29	time-invariant (29 °C)	yes	yes
SST27	time-invariant (27 °C)	yes	yes
SST31	time-invariant (31 °C)	yes	yes
SST29D1	diurnally-varied with mean of 29 °C and maximum diurnal difference of 1 °C	yes	yes
SST29D2	diurnally-varied with mean of 29 °C and maximum diurnal difference of 2 °C	yes	yes
SST29NCR	time-invariant (29 °C)	no for both water and ice clouds	yes
SST29NIR	time-invariant (29 °C)	no for ice clouds	yes
SST29NWR	time-invariant (29 °C)	no for water clouds	yes
SST29NIM	time-invariant (29 °C)	no for ice clouds	no

The model predicts temperature through cloud–radiation interaction using solar and thermal infrared radiation parameterization schemes,[41–43] water vapor, perturbation zonal wind, and vertical velocity. The model also predicts cloud water q_c, raindrops q_r, cloud ice q_i, snow q_s, and graupel q_g using the single-moment cloud microphysical parameterization scheme.[44–48] The model is furnished with cyclic lateral boundary conditions. The basic model parameters include a model domain of 768 km with a horizontal grid mesh of 1.5 km, 33 vertical layers, and a time step of 12 s. Detailed model setup and physics can be found in Refs. [15] and [49].

3. Relationships between RMPE, CMPE, and LSPE

Following Gao and Li,[12] RMPE, CMPE, and LSPE can be respectively defined as

$$E_{\mathrm{RM}} = P_{\mathrm{S}}/S_{\mathrm{RB}}, \tag{1a}$$

$$E_{\mathrm{CM}} = P_{\mathrm{S}}/S_{\mathrm{CB}}, \tag{1b}$$

$$E_{\mathrm{LS}} = P_{\mathrm{S}}/S_{\mathrm{WVCB}}, \tag{1c}$$

where

$$S_{\mathrm{RB}} = \sum_{I=1}^{12} H(P_{I\mathrm{R}})P_{I\mathrm{R}} + H(Q_{\mathrm{RM}})Q_{\mathrm{RM}}, \tag{2a}$$

$$S_{\mathrm{CB}} = \sum_{I=1}^{7} H(P_I)P_I + H(Q_{\mathrm{CM}})Q_{\mathrm{CM}}, \tag{2b}$$

$$\begin{aligned} S_{\mathrm{WVCB}} = {} & H(Q_{\mathrm{WVT}})Q_{\mathrm{WVT}} + H(Q_{\mathrm{WVF}})Q_{\mathrm{WVF}} \\ & + H(Q_{\mathrm{WVE}})Q_{\mathrm{WVE}} + H(Q_{\mathrm{CM}})Q_{\mathrm{CM}}, \end{aligned} \tag{2c}$$

$$\begin{aligned} P_{I\mathrm{R}} = {} & ([P_{\mathrm{SACW}}(T > T_{\mathrm{o}})], [P_{\mathrm{RAUT}}], [P_{\mathrm{RACW}}], \\ & [P_{\mathrm{GACW}}(T > T_{\mathrm{o}})], -[P_{\mathrm{REVP}}], [P_{\mathrm{RACS}}(T > T_{\mathrm{o}})], \\ & -[P_{\mathrm{IACR}}(T < T_{\mathrm{o}})], -[P_{\mathrm{GACR}}(T < T_{\mathrm{o}})], \\ & -[P_{\mathrm{SACR}}(T < T_{\mathrm{o}})], -[P_{\mathrm{GFR}}(T < T_{\mathrm{o}})], \\ & [P_{\mathrm{SMLT}}(T > T_{\mathrm{o}})], [P_{\mathrm{GMLT}}(T > T_{\mathrm{o}})]), \end{aligned} \tag{2d}$$

$$\begin{aligned} P_I = {} & ([P_{\mathrm{CND}}], [P_{\mathrm{DEP}}], [P_{\mathrm{SDEP}}], [P_{\mathrm{GDEP}}], \\ & -[P_{\mathrm{REVP}}], -[P_{\mathrm{MLTG}}], -[P_{\mathrm{MLTS}}]), \end{aligned} \tag{2e}$$

$$Q_{\mathrm{RM}} = -\frac{\partial [q_{\mathrm{r}}]}{\partial t} - \left[u\frac{\partial q_{\mathrm{r}}}{\partial x}\right] - \left[w\frac{\partial q_{\mathrm{r}}}{\partial z}\right], \tag{2f}$$

$$Q_{\mathrm{CM}} = -\frac{\partial [q_5]}{\partial t} - \left[u\frac{\partial q_5}{\partial x}\right] - \left[w\frac{\partial q_5}{\partial z}\right], \tag{2g}$$

$$Q_{\mathrm{WVT}} = -\frac{\partial [q_v]}{\partial t}, \tag{2h}$$

$$\begin{aligned} Q_{\mathrm{WVF}} = {} & -\left[\bar{u}^o\frac{\partial \bar{q}_v}{\partial x}\right] - \left[\frac{\partial (u'q'_v)}{\partial x}\right] \\ & - \left[\bar{u}^o\frac{\partial q'_v}{\partial x}\right] - \left[w'\frac{\partial \bar{q}_v}{\partial z}\right], \end{aligned} \tag{2i}$$

$$Q_{\mathrm{WVE}} = E_{\mathrm{s}}. \tag{2j}$$

Here, P_{S} is the surface rain rate; u and w are the zonal and vertical components of wind, respectively; $P_{I\mathrm{R}}$ denotes rainfall source/sink terms from the rain microphysical process, and P_I denotes rainfall source/sink terms from the cloud microphys-

ical process shown in Table 2; q_v is the water vapor mixing ratio; $q_5 = q_c + q_r + q_i + q_s + q_g$; E_s is the surface evaporation rate; $T_o = 0\ ^\circ$C; overbar is domain mean, and prime is the perturbation from the domain mean; superscript o denotes the imposed variable in the model; $[()] = \int_{z_b}^{z_t} \bar{\rho}()\,\mathrm{d}z$, z_t and z_b are the heights of the top and the bottom of the model atmosphere, respectively; S_{RB}, S_{CB}, and S_{WVCB} are the rainfall sources from rain, cloud, and surface rainfall budgets, respectively; H is the Heaviside function, $H(F) = 1$ when $F > 0$, and $H(F) = 0$ when $F \leq 0$. The rainfall sources are calculated by accumulating rainfall sources from each model grid over the model domain.

Table 2. List of microphysical processes and their parameterization schemes. The schemes are given by Lin *et al.* (1983, LFO), Rutledge and Hobbs (1983; 1984; RH83, RH84), Tao *et al*. (1989, TSM), and Krueger *et al*. (1995, KFLC).

Notation	Description	Scheme
P_{MLTG}	growth of vapor by evaporation of liquid from graupel surface	RH84
P_{MLTS}	growth of vapor by evaporation of melting snow	RH83
P_{REVP}	growth of vapor by evaporation of raindrops	RH83
P_{IMLT}	growth of cloud water by melting of cloud ice	RH83
P_{CND}	growth of cloud water by condensation of supersaturated vapor	TSM
P_{GMLT}	growth of raindrops by melting of graupel	RH84
P_{SMLT}	growth of raindrops by melting of snow	RH83
P_{RACI}	growth of raindrops by the accretion of cloud ice	RH84
P_{RACW}	growth of raindrops by the collection of cloud water	RH83
P_{RACS}	growth of raindrops by the accretion of snow	RH84
P_{RAUT}	growth of raindrops by the autoconversion of cloud water	LFO
P_{IDW}	growth of cloud ice by the deposition of cloud water	KFLC
P_{IACR}	growth of cloud ice by the accretion of rain	RH84
P_{IHOM}	growth of cloud ice by the homogeneous freezing of cloud water	
P_{DEP}	growth of cloud ice by the deposition of supersaturated vapor	TSM
P_{SAUT}	growth of snow by the conversion of cloud ice	RH83
P_{SACI}	growth of snow by the collection of cloud ice	RH83
P_{SACW}	growth of snow by the accretion of cloud water	RH83
P_{SFW}	growth of snow by the deposition of cloud water	KFLC
P_{SFI}	depositional growth of snow from cloud ice	KFLC
P_{SACR}	growth of snow by the accretion of raindrops	LFO
P_{SDEP}	growth of snow by the deposition of vapor	RH83
P_{GACI}	growth of graupel by the collection of cloud ice	RH84
P_{GACR}	growth of graupel by the accretion of raindrops	RH84
P_{GACS}	growth of graupel by the accretion of snow	RH84
P_{GACW}	growth of graupel by the accretion of cloud water	RH84
P_{WACS}	growth of graupel by the riming of snow	RH84
P_{GDEP}	growth of graupel by the deposition of vapor	RH84
P_{GFR}	growth of graupel by the freezing of raindrops	LFO

Figure 1(a) shows the following relationship among RMPE, CMPE, and LSPE in the control experiment:

$$E_{RM} > E_{CM} > E_{LS}, \tag{3}$$

which is similar to that found by Gao and Li,[12] though the model is driven without large-scale vertical velocity in this study.

In the cloud microphysical budget, Eq. (2b) becomes

$$S_{CB} = S_{RB} + S_{CWCISGB}, \tag{4}$$

where

$$\begin{aligned} S_{CWCISGB} = & \sum_{I=1}^{9} H(P_{ICW})P_{ICW} + H(Q_{CWM})Q_{CWM} \\ & + \sum_{I=1}^{9} H(P_{ICI})P_{ICI} + H(Q_{CIM})Q_{CIM} \\ & + \sum_{I=1}^{15} H(P_{IS})P_{IS} + H(Q_{SM})Q_{SM} \\ & + \sum_{I=1}^{14} H(P_{IG})P_{IG} + H(Q_{GM})Q_{GM}, \end{aligned} \tag{5}$$

$$\begin{aligned} P_{ICW} = & (-P_{SACW}, -P_{RAUT}, -P_{RACW}, -P_{SFW}(T < T_o), \\ & - P_{GACW}, P_{CND}, -P_{IHOM}(T < T_{oo}), P_{IMLT}(T > T_o), \\ & - P_{IDW}(T_{oo} < T < T_o)), \end{aligned} \tag{5a}$$

$$\begin{aligned} P_{ICI} = & (-P_{SAUT}(T < T_o), -P_{SACI}(T < T_o), -P_{RACI}(T < T_o), \\ & - P_{SFI}(T < T_o), -P_{GACI}(T < T_o), P_{IHOM}(T < T_{oo}), \\ & - P_{IMLT}(T > T_o), P_{IDW}(T_{oo} < T < T_o, P_{DEP})), \end{aligned} \tag{5b}$$

$$\begin{aligned} P_{IS} = & (P_{SAUT}(T < T_o), P_{SACI}(T < T_o), P_{SACW}(T < T_o), \\ & P_{SFW}(T < T_o), P_{SFI}(T < T_o), P_{RACI}(T < T_o), \end{aligned}$$

$$
\begin{aligned}
&-P_{\mathrm{RACS}}(T>T_{\mathrm{o}}),-P_{\mathrm{GACS}},-P_{\mathrm{SMLT}}(T>T_{\mathrm{o}}),\\
&-P_{\mathrm{RACS}}(T<T_{\mathrm{o}}),P_{\mathrm{SACR}}(T<T_{\mathrm{o}}),\\
&P_{\mathrm{SDEP}}(T<T_{\mathrm{o}}),-P_{\mathrm{MLTS}}(T>T_{\mathrm{o}}),\\
&P_{\mathrm{IACR}}(T<T_{\mathrm{o}}),-P_{\mathrm{WACS}}(T<T_{\mathrm{o}})), \qquad (5c)\\
P_{I\mathrm{G}} = &(P_{\mathrm{RACI}}(T<T_{\mathrm{o}}),P_{\mathrm{GACI}}(T<T_{\mathrm{o}}),\\
&P_{\mathrm{GACW}}(T<T_{\mathrm{o}}),P_{\mathrm{SACW}}(T<T_{\mathrm{o}}),P_{\mathrm{GACS}},\\
&P_{\mathrm{IACR}}(T<T_{\mathrm{o}}),P_{\mathrm{GACR}}(T<T_{\mathrm{o}}),\\
&P_{\mathrm{RACS}}(T<T_{\mathrm{o}}),P_{\mathrm{GFR}}(T<T_{\mathrm{o}}),\\
&P_{\mathrm{WACS}}(T<T_{\mathrm{o}}),-P_{\mathrm{GMLT}}(T>T_{\mathrm{o}}),\\
&P_{\mathrm{GDEP}}(T<T_{\mathrm{o}}),-P_{\mathrm{MLTG}}(T>T_{\mathrm{o}}),\\
&P_{\mathrm{SACR}}(T<T_{\mathrm{o}})), \qquad (5d)
\end{aligned}
$$

$$Q_{\mathrm{CWM}} = -\frac{\partial[q_{\mathrm{c}}]}{\partial t} - \left[u\frac{\partial q_{\mathrm{c}}}{\partial x}\right] - \left[w\frac{\partial q_{\mathrm{c}}}{\partial z}\right], \qquad (5e)$$

$$Q_{\mathrm{CIM}} = -\frac{\partial[q_{\mathrm{i}}]}{\partial t} - \left[u\frac{\partial q_{\mathrm{i}}}{\partial x}\right] - \left[w\frac{\partial q_{\mathrm{i}}}{\partial z}\right], \qquad (5f)$$

$$Q_{\mathrm{SM}} = -\frac{\partial[q_{\mathrm{s}}]}{\partial t} - \left[u\frac{\partial q_{\mathrm{s}}}{\partial x}\right] - \left[w\frac{\partial q_{\mathrm{s}}}{\partial z}\right], \qquad (5g)$$

$$Q_{\mathrm{GM}} = -\frac{\partial[q_{\mathrm{g}}]}{\partial t} - \left[u\frac{\partial q_{\mathrm{g}}}{\partial x}\right] - \left[w\frac{\partial q_{\mathrm{g}}}{\partial z}\right]. \qquad (5h)$$

Here, $P_{I\mathrm{CW}}$, $P_{I\mathrm{CI}}$, $P_{I\mathrm{S}}$, and $P_{I\mathrm{G}}$ denote the rainfall source/sink terms from cloud water, cloud ice, snow, and graupel microphysical processes, respectively, and P_I denotes the rainfall source/sink terms from the cloud microphysical process shown in Table 2.

Since it consists of positive values only, S_{CWCISGB} is always positive because the rainfall is generally associated with cloud water and ice microphysical processes, which are sources for rainfall. Thus, S_{CB} is larger than S_{RB} as indicated in Fig. 1(b).

From Eqs. (1a) and (1b), we have

$$\frac{E_{\mathrm{RM}}}{E_{\mathrm{CM}}} = \frac{S_{\mathrm{CB}}}{S_{\mathrm{RB}}} > 0. \qquad (6)$$

Equations (2b) and (2c) show a common item $(H(Q_{\mathrm{CM}})Q_{\mathrm{CM}})$. Thus, S_{WVCB} and S_{CB} come from the water vapor budget. The S_{WVCB} is a cloud source for S_{CB}. As a result, we have the following relation:

$$S_{\mathrm{WVCB}} \geq S_{\mathrm{CB}}. \qquad (7)$$

Due to the cyclic lateral boundaries, the water vapor convergence over rainfall regions is offset by the water vapor divergence over rainfall-free regions in the control experiment.[14] Since the evaporation of rain only occurs over cloudy regions, its magnitude may be smaller than that of the water vapor divergence. Therefore, S_{WVCB} is much larger than S_{CB} (Fig. 1(b)). From Eqs. (1b) and (1c), we have

$$\frac{E_{\mathrm{CM}}}{E_{\mathrm{LS}}} = \frac{S_{\mathrm{WVCB}}}{S_{\mathrm{CB}}} > 0. \qquad (8)$$

Inequalities (6) and (8) lead to inequality (3).

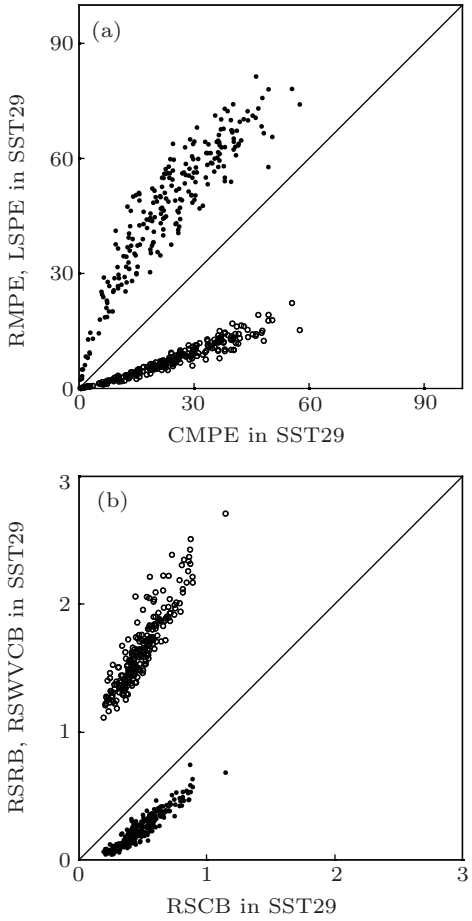

Fig. 1. (a) CMPE versus RMPE (solid circle) and LSPE (open circle) and (b) RSCB versus RSRB (solid circle) and RSWVCB (open circle). Units are mm·h^{-1} for RSRB, RSCB, and RSWVCB, and % for RMPE, CMPE, and LSPE. The straight line denotes CMPE = RMPE and CMPE = LSPE in panel (a), whereas it denotes RSCB (S_{CB}) = RSRB (S_{RB}) and RSCB = RSWVCB (S_{WVCB}) in panel (b).

4. Effects of SST, diurnal variation, and clouds on precipitation efficiency

Figure 2 reveals that the differences in PE between SST29 and SST27, SST29D1 and SST29, and SST29NIR and SST29 are negatively correlated with those between SST31 and SST29, SST29D2 and SST29D1, and SST29NIM and SST29NIR with the correlation coefficients larger than −0.39. The student's t-test on the significance of the correlation coefficients is conducted and the critical correlation coefficient at 1% significant level is 0.19. Thus, the negative correlations are statistically significant. The effect of the increase in the SST from 27 °C to 29 °C on PE is opposite to the effect of the SST increasing from 29 °C to 31 °C on PE. The inclusion of diurnal variation of the SST with the diurnal difference of 1 °C and the 1 °C increase in the diurnal difference from SST29D1 to SST29D2 can cause an opposite change of PE. The inclusion of radiative and microphysical effects of ice clouds can generate an opposite effect on PE. The differences in PE for SST29NCR–SST29NIR and SST29NWR–SST29 do not show a statistically significant correlation since their correlation coefficients are about zero. This indicates that the radia-

tive effects of ice clouds do not dominantly affect the radiative effects of water clouds on PE. The correlation coefficients of PEs are similar, though the differences in LSPE are much less than those in RMPE and CMPE. The variations of differences in PE between the positive and the negative values are caused by the diurnal variation of radiation in all experiments.

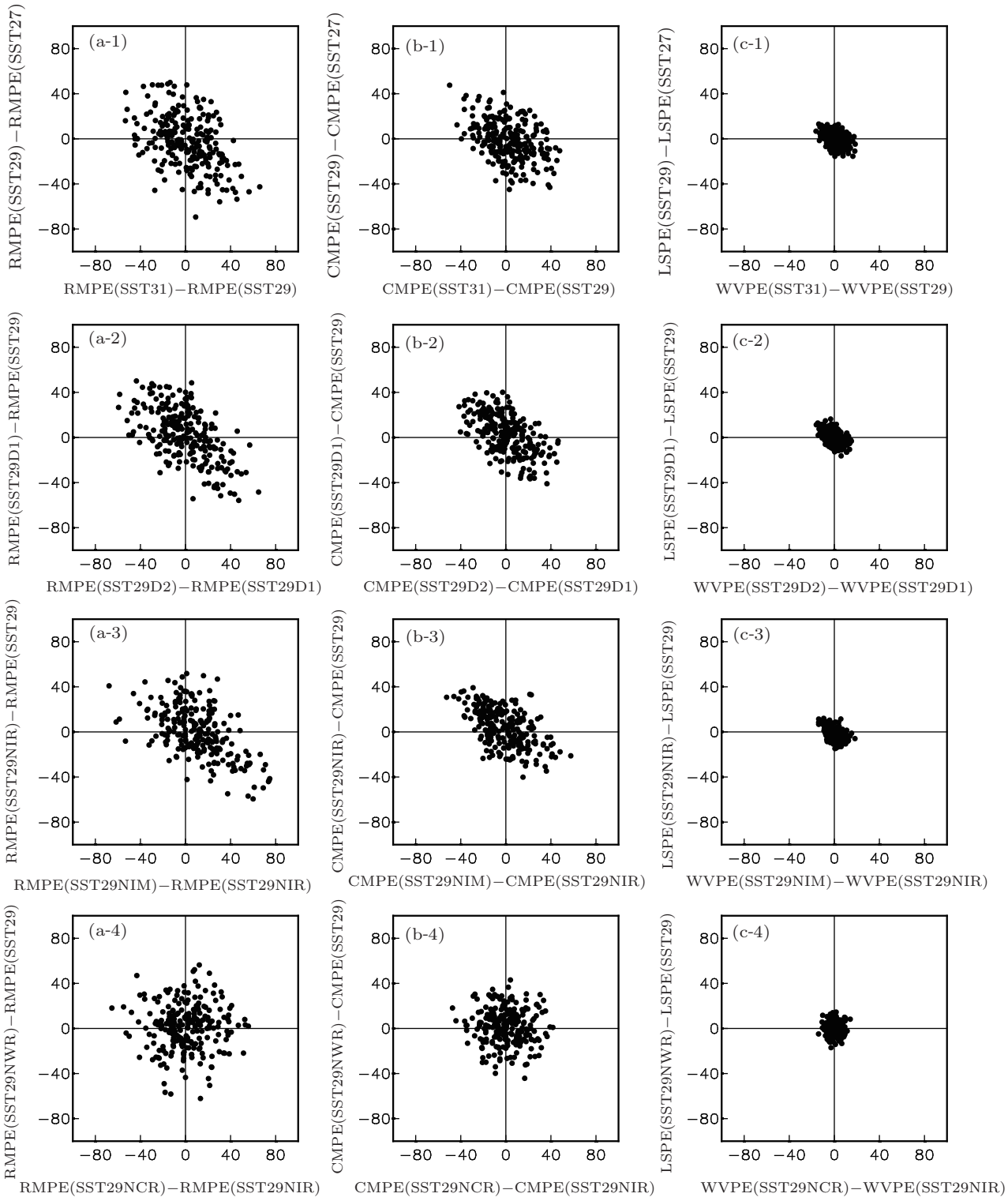

Fig. 2. (1) Differences in PE for SST29–SST27 versus difference in PE for SST31–SST29, (2) differences in PE for SST29D1-SST29 versus difference in PE for SST29D2–SST29D1, (3) differences in PE for SST29NIR–SST29 versus difference in PE for SST29NIM–SST29NIR, and (4) differences in PE for SST29NWR–SST29 versus difference in PE for SST29NCR–SST29NIR. PEs are RMPE in panel (a), CMPE in panel (b), and LSPE in panel (c). Units are %.

Figure 3 shows that the differences in rain rate between SST29 and SST27, SST29D1 and SST29, and SST29NIR and SST29 are negatively correlated with those between SST31 and SST29, SST29D2 and SST29D1, and SST29NIM and SST29NIR with the correlation coefficients larger than −0.36. The difference in rain rate for SST29NCR and SST29CIR is not correlated with that for SST29NWR and SST29 since their correlation coefficient is about zero. The comparison between Figs. 2 and 3 and the similarities of correlation coefficients imply that the difference in PE is associated with the difference in rain rate.

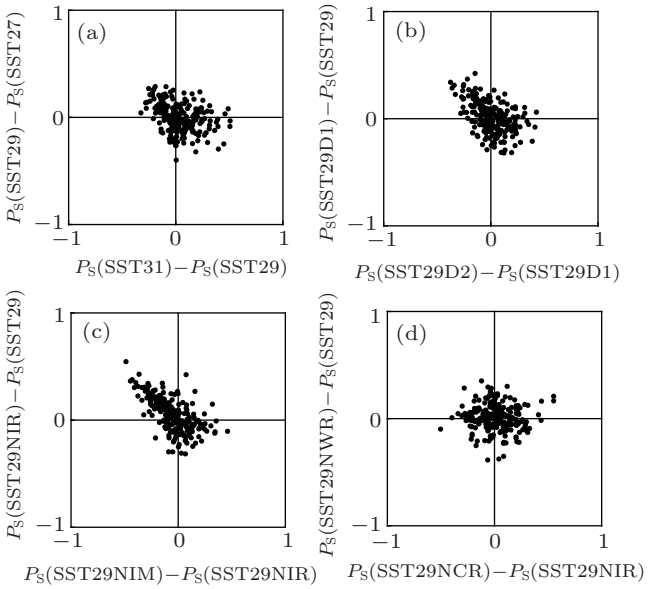

Fig. 3. (a) Difference in P_S between SST29 and SST27 versus difference in P_S between SST31 and SST29, (b) difference in P_S between SST29D1 and SST29 versus difference in P_S between SST29D2 and SST29D1, (c) difference in P_S between SST29NIR and SST29 versus difference in P_S between SST29NIM and SST29NIR, and (d) difference in P_S between SST29NWR and SST29 versus difference in P_S between SST29NCR and SST29NIR. Units are mm·h^{-1}.

The exclusion of radiative effects of ice clouds lowers the saturation mixing ratio by falling air temperature, thereby enhancing the condensation and thus the rainfall, whereas the removal of the microphysical effect of ice clouds reduces the rainfall through the exclusion of deposition. Thus, the elimination of radiative and microphysical effects of ice clouds causes an opposite change of rainfall and thus the precipitation efficiency. The diurnal variation of rainfall stems from the diurnal variation of radiation associated with the diurnal variation of solar zenith angle.[50] For other three pairs of differences in rain rate, we examine the difference in radiation since diurnal signals prevail in these sensitivity experiments. Figure 4 reveals statistically significant negative correlations between the S_{RAD} (mass-weighted mean radiation) differences for SST29–SST27 and SST31 and SST29 and for SST29D1–SST29 and SST29D2–SST29D1. This implies that the negative correlation between the differences in rain rate is associated with that in radiation in these sensitivity experiments. The difference in radiation for SST29NWR–SST29 is not statistically significantly correlated with that for SST29NCR–SST29NIR, which accounts for the statistically significant correlation for rain rate and thus for PE.

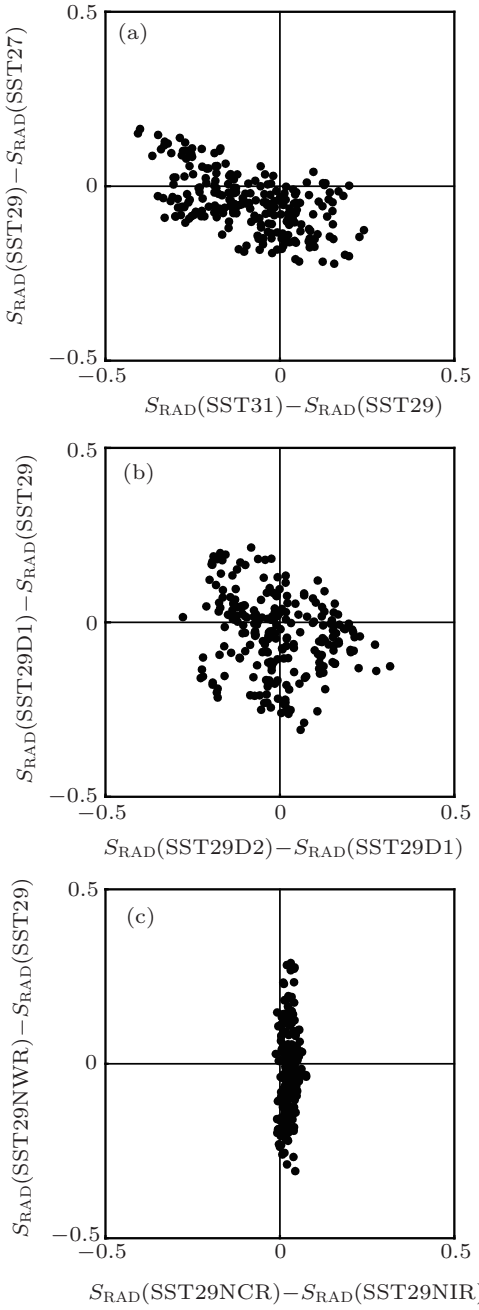

Fig. 4. (a) Difference in S_{RAD} (in units of °C·d^{-1}) between SST29 and SST27 versus difference in S_{RAD} between SST31 and SST29, (b) difference in S_{RAD} between SST29D1 and SST29 versus difference in S_{RAD} between SST29D2 and SST29D1, and (c) difference in S_{RAD} between SST29NWR and SST29 versus difference in S_{RAD} between SST29NCR and SST29NIR.

The negative correlations between the radiation differences for SST29–SST27 and SST31–SST29 (Fig. 4(a)), and for SST29D1–SST29 and SST29D2–SST29D1 (Fig. 4(b)) show the positive radiation difference for SST29–SST27 with the negative radiation difference for SST31–SST29, the negative radiation difference for SST29–SST27 with the positive

radiation difference for SST31–SST29, the positive radiation difference for SST29D1–SST29 with the negative radiation difference for SST29D2–SST29D1, and the negative radiation difference for SST29D1–SST29 with the positive radiation difference for SST29D2–SST29D1. The positive radiation difference for SST29–SST27 with the negative radiation difference for SST31–SST29 covers 23% of the analysis period and 55% occurs during the night time (1900–0600 local standard time), whereas the negative radiation difference for SST29–SST27 with the positive radiation difference for SST31–SST29 occupies 30% of the analysis period and 47% appears during the night time. The positive radiation difference for SST29–SST27 is mainly determined by the positive difference in infrared radiation from 11 km to 16 km and the solar radiation from 15 km to 18 km, while the negative radiation difference for SST31–SST29 is mainly induced by the negative difference in infrared radiation from 9 km to 16 km (Fig. 5). The negative radiation difference for SST29–SST27 is accounted for by the negative difference in infrared radiation from 8 km to 17 km, and the positive radiation difference for SST31–SST29 is primarily determined by the positive difference in infrared radiation around 14–16 km and the positive difference in solar radiation around 12–17 km. The effects of 2 °C increase from 27 °C to 29 °C and 29 °C to 31 °C on rainfall could be opposite, and the differences in infrared and solar radiations generally occur above 6 km where the ice clouds dominate.

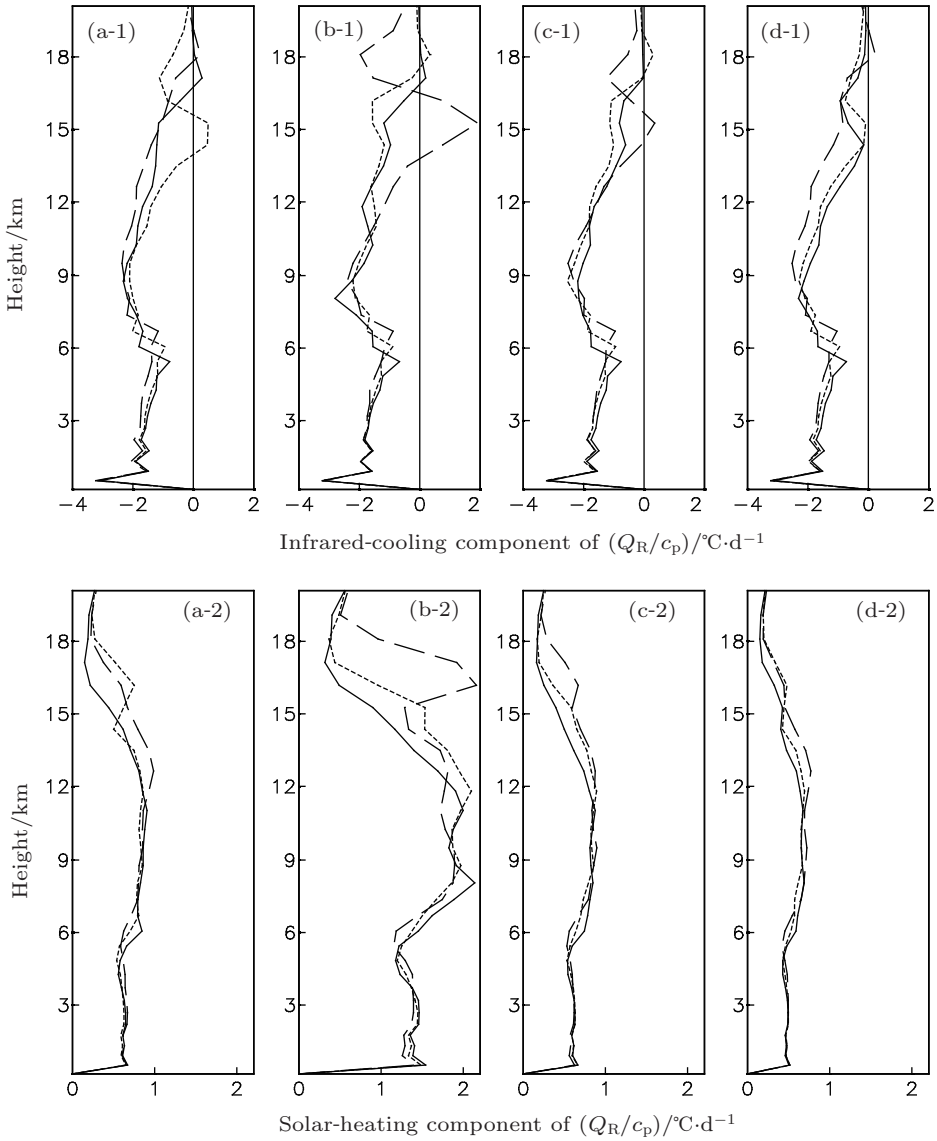

Fig. 5. Composites of vertical profiles of (1) infrared and (2) solar radiations in SST27 (solid), SST29 (short dash), and SST31 (long dash) for (a) positive S_{RAD} for SST29–SST27 and negative S_{RAD} for SST31–SST29, (b) positive S_{RAD} for SST29–SST27 and positive S_{RAD} for SST31–SST29, (c) negative S_{RAD} for SST29–SST27 and positive S_{RAD} for SST31–SST29, (d) negative S_{RAD} for SST29–SST27 and negative S_{RAD} for SST31–SST29.

The positive radiation difference for SST29D1–SST29 with the negative radiation difference for SST29D2–SST29D1 covers 32% of the analysis period and 58% occurs during the night time, whereas the negative radiation difference for SST29D1–SST29 with the positive radiation difference for SST29D2–SST29D1 occupies 31% of the analysis period and 60% appears during the night time. The positive difference in infrared radiation for SST29D1–SST29 around 15 km primarily accounts for the positive radiation difference, whereas the negative differences in infrared radiation from 9 km to 16 km and the solar radiation from 14 km to 18 km mainly contribute to the negative radiation difference for SST29D2–SST29D1 (Fig. 6). The negative differences in infrared radiation from 8 km to 16 km and the solar radiation from 15 km to 18 km cause the negative radiation difference for SST29D1–SST29, whereas the positive difference in infrared radiation from 8 km to 16 km primarily determines the positive radiation difference for SST29D2–SST29D1.

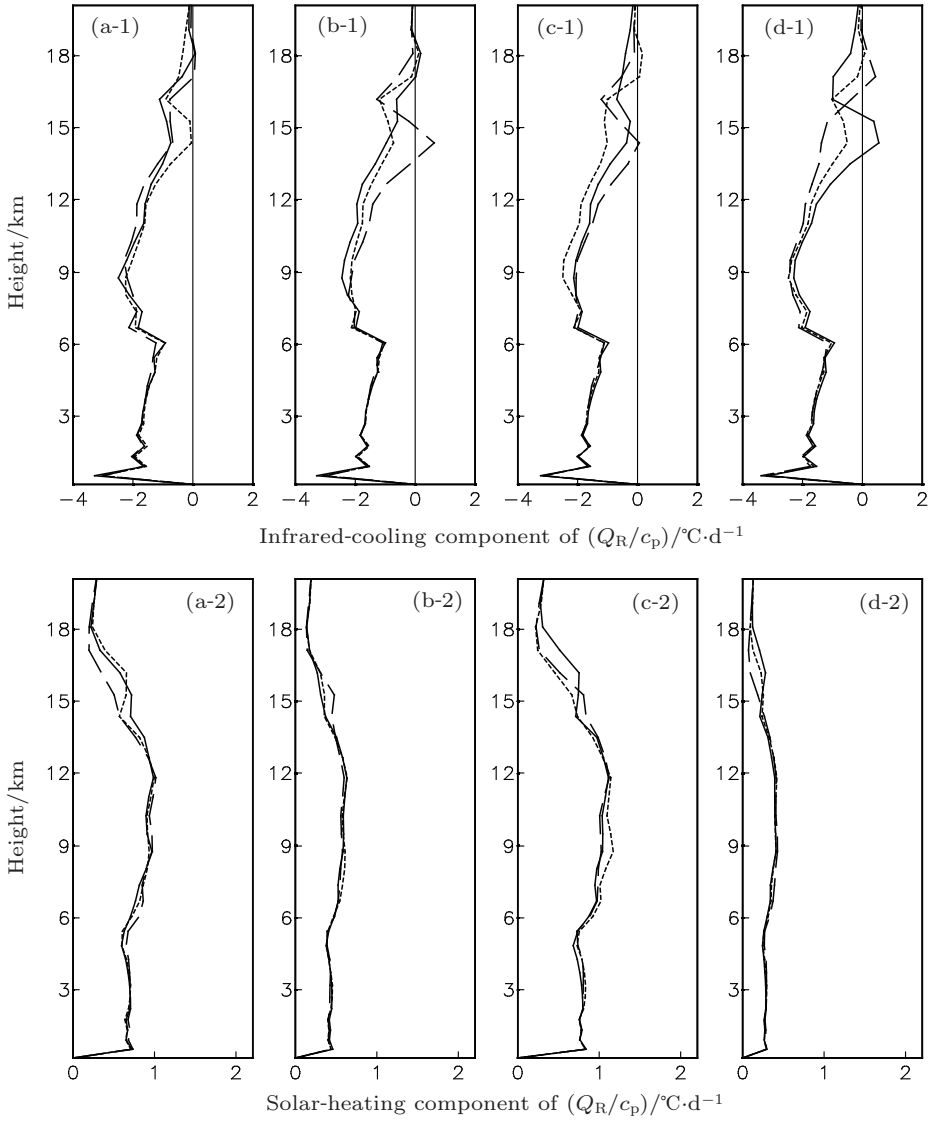

Fig. 6. Composites of vertical profiles of (1) infrared and (2) solar radiations in SST29 (solid), SST29D1 (short dash), and SST29D2 (long dash) for (a) positive S_{RAD} for SST29D1–SST29 and negative S_{RAD} for SST29D2–SST29D1, (b) positive S_{RAD} for SST29D1–SST29 and positive S_{RAD} for SST29D2–SST29D1, (c) negative S_{RAD} for SST29D1–SST29 and positive S_{RAD} for SST29D2–SST29D1, (d) negative S_{RAD} for SST29D1–SST29 and negative S_{RAD} for SST29D2–SST29D1.

This indicates that the effects of increased SST and strengthened diurnal SST difference on the precipitation efficiency depend on the ice cloud–radiation interactions. The crucial roles of ice clouds that play in the cloud–radiation interaction processes indicate that precipitation modeling requires accurate estimates of the ice clouds from the ice microphysical parameterization scheme and the cloud–radiation interaction form the radiation parameterization scheme.

5. Summary

The effects of sea surface temperature and its diurnal variation radiation and clouds on precipitation efficiency are examined by using grid-scale data from a series of two-dimensional equilibrium sensitivity cloud-resolving model experiments. The major results are as follows.

1) The precipitation efficiency defined in the cloud microphysical budget is higher than that defined in the surface rainfall budget, but is lower than that defined in the rain microphysical budget. The former is physically proved, whereas the latter is mathematically demonstrated.

2) The difference in precipitation efficiency caused by the 2 °C increase from 27 °C to 29 °C is negatively correlated with that from 29 °C to 31 °C. The difference in precipitation efficiency caused by the inclusion of diurnal difference 1 °C and that caused by the 1 °C increase in diurnal difference also show a negative correlation. The negative correlation is explained by the negative correlation in radiation, which is largely associated with the ice clouds.

3) The difference in precipitation efficiency resulting from the exclusion of the radiative effect of ice clouds is negatively correlated with that from the removal of microphysical effect of ice clouds, because the exclusion of the radiative effect of ice clouds tends to increase rainfall by reducing the saturation mixing ratio whereas the elimination of microphysical effect of ice clouds tends to enhance rainfall by cutting net condensation.

4) The difference in precipitation efficiency caused by the exclusion of the radiative effect of water effect in the presence of radiative effect of ice clouds and that in the absence of radiative effect of ice clouds do not show any correlation. This indicates that the radiative effect of water clouds on precipitation efficiency is statistically independent of the radiative effects of ice clouds.

Although the experimental data of a two-dimensional model are used for this analysis, the mathematical and physical demonstration of the relationships among precipitation efficiencies defined in the different budgets are not related to dimensionality. Nevertheless, the experiments of three-dimensional cloud-resolving models may be further conducted to validate the effects of clouds, sea surface temperature, and diurnal variation on the precipitation efficiency.

Acknowledgment

The authors thank Dr. Tao W K at NASA/GSFC for his two-dimensional cloud-resolving model, and Dr Gao S and Dr Ping F at the Institute of Atmospheric Physics, Chinese Academy of Sciences for their model simulation data.

References

[1] Auer A H Jr and Marwitz J D 1968 *J. Appl. Meteor.* **7** 196
[2] Weisman M L and Klemp J B 1982 *Mon. Wea. Rev.* **110** 504
[3] Heymsfield G M and Schotz S 1985 *Mon. Wea. Rev.* **113** 1563
[4] Lipps F B and Hemler R S 1986 *J. Atmos. Sci.* **43** 1796
[5] Chong M and Hauser D 1989 *Mon. Wea. Rev.* **117** 728
[6] Doswell C A, Brooks H E and Maddox R A 1996 *Wea. Forecasting* **11** 560
[7] Li X, Sui C H and Lau K M 2002 *J. Meteor. Soc. Jpn.* **80** 205
[8] Sui C H, Li X, Yang M J and Huang H L 2005 *J. Atmos. Sci.* **62** 4358
[9] Braham R R Jr 1952 *J. Meteor.* **9** 227
[10] Sui C H, Li X and Yang M J 2007 *J. Atmos. Sci.* **64** 4506
[11] Gao S, Cui X, Zhou Y and Li X 2005 *J. Geophys. Res.* **110** D10202
[12] Gao S and Li X 2011 *Quart. J. Roy. Meteor. Soc.* **137** 969
[13] Ping F, Luo Z and Li X 2007 *Mon. Wea. Rev.* **135** 2794
[14] Zhou Y and Li X 2009 *Atmos. Res.* **92** 212
[15] Gao S and Li X 2008 *Cloud-resolving Modeling of Convective Processes* (Berlin: Springer) pp. 1–206
[16] Gao S, Zhou Y and Li X 2007 *J. Atmos. Sci.* **64** 656
[17] Gao S 2008 *J. Geophys. Res.* **113** D03108
[18] Soong S T and Ogura Y 1980 *J. Atmos. Sci.* **37** 2035
[19] Soong S T and Tao W K 1980 *J. Atmos. Sci.* **37** 2016
[20] Tao W K and Simpson J 1993 *Terr. Atmos. Oceanic Sci.* **4** 35
[21] Li X, Sui C H, Lau K M and Chou M D 1999 *J. Atmos. Sci.* **56** 3028
[22] Li X, Sui C H and Lau K M 2002 *Mon. Wea. Rev.* **130** 2481
[23] Sui C H, Lau K M, Tao W K and Simpson J 1994 *J. Atmos. Sci.* **51** 711
[24] Sui C H, Li X and Lau K M 1998 *J. Atmos. Sci.***55** 2345
[25] Tao W K and Soong S T 1986 *J. Atmos. Sci.***43** 2653
[26] Tao W K, Simpson J and Soong S T 1987 *J. Atmos. Sci.***44** 3175
[27] Grabowski W W, Wu X, Moncrieff M W and Hall W D 1998 *J. Atmos. Sci.* **55** 3264
[28] Tompkins A M 2000 *Mon. Wea. Rev.* **128** 1521
[29] Khairoutdinov M F and Randall D A 2003 *J. Atmos. Sci.* **60** 607
[30] Zhou Y and Li X 2011 *Adv. Atmos. Sci.* **28** 1099
[31] Jiang Z, Li X, Zhou Y and Gao S 2012 *Chin. Phys. B* **21** 054215
[32] Cui X 2008 *J. Geophys. Res.* **113** D02113
[33] Cui X and Li X 2009 *Meteor. Atmos. Phys.* **104** 53
[34] Cui X and Li X 2011 *Chin. Phys. B* **20** 109201
[35] Ping F and Luo Z 2009 *Atmos. Res.* **93** 862
[36] Cui X and Li X 2006 *J. Geophys. Res.* **111** D17112
[37] Li X and Zou CZ 2009 *Meteor. Atmos. Phys.* **105** 85
[38] Ping F, Luo Z and Li X 2011 *Meteor Atmos Phys* **112** 29
[39] Ping F, Luo Z and Wang H 2011 *Atmos. Sci. Lett.* **12** 300
[40] Zhou Y and Li X 2012 *J. Tropical Meteor.* **18** 369
[41] Chou M D and Suarez M J 1994 *NASA Tech. Memo.* **104606** 3
[42] Chou M D, Kratz D P and Ridgway W 1991 *J. Climate* **4** 424
[43] Chou M D, Suarez M J, Ho C H, Yan M M H and Lee K T 1998 *J. Climate* **11** 202
[44] Lin Y L, Farley R D and Orville H D 1983 *J. Climate Appl. Meteor.* **22** 1065
[45] Rutledge S A and Hobbs R V 1983 *J. Atmos. Sci.* **40** 1185
[46] Rutledge S A and Hobbs R V 1984 *J. Atmos. Sci.* **41** 2949
[47] Tao W K, Simpson J and McCumber M 1989 *Mon. Wea. Rev.* **117** 231
[48] Krueger S K, Fu Q, Liou K N and Chin H N S 1995 *J. Appl. Meteor.* **34** 281
[49] Li X and Gao S 2011 *Precipitation Modeling and Quantitative Analysis*. (Berlin: Springer) pp. 1–240
[50] Ga S and Li X 2010 *J. Geophys. Res.* **115** D08204